PB84-162601

Determination of Cloud Parameters for NEROS II from Digital Satellite Data

Colorado State Univ., Fort Collins

Prepared for

Environmental Sciences Research Lab.
Research Triangle Park, NC

Mar 84

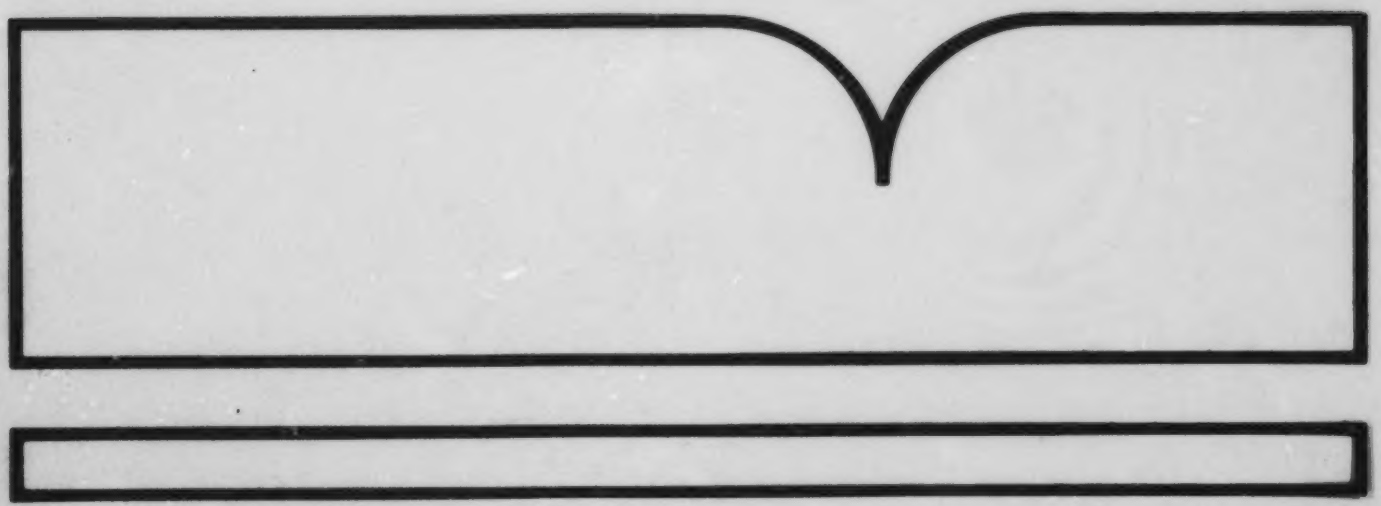

U.S. Department of Commerce
National Technical Information Service
NTIS

PB84-162601

EPA-600/3-84-044
March 1984

DETERMINATION OF CLOUD PARAMETERS FOR NEROS II FROM DIGITAL SATELLITE DATA

by
Jan L. Behunek
Thomas H. Vonder Haar
Pat Laybe

Department of Atmospheric Science
Colorado State University
Fort Collins, Colorado 80523

EPA Contract No. 68-02-3731

Project Officer:

Terry L. Clark
Meteorology and Assessment Division
Environmental Sciences Research Laboratory
U.S. Environmental Protection Agency
Research Triangle Park, North Carolina 27711

ENVIRONMENTAL SCIENCES RESEARCH LABORATORY
OFFICE OF RESEARCH AND DEVELOPMENT
U.S. ENVIRONMENTAL PROTECTION AGENCY
RESEARCH TRIANGLE PARK, NORTH CAROLINA 27711

REPRODUCED BY
NATIONAL TECHNICAL
INFORMATION SERVICE
U.S. DEPARTMENT OF COMMERCE
SPRINGFIELD, VA. 22161

TECHNICAL REPORT DATA
(Please read Instructions on the reverse before completing)

1. REPORT NO.	2.	3. RECIPIENT'S ACCESSION NO.
EPA-600/3-84-044		PB84 162601

4. TITLE AND SUBTITLE	5. REPORT DATE
DETERMINATION OF CLOUD PARAMETERS FOR NEROS II FROM DIGITAL SATELLITE DATA	March 1984
	6. PERFORMING ORGANIZATION CODE
7. AUTHOR(S)	8. PERFORMING ORGANIZATION REPORT NO.
Jan. L. Behunek, T. H. Vonder Haar, and Pat Laybe	
9. PERFORMING ORGANIZATION NAME AND ADDRESS	10. PROGRAM ELEMENT NO.
Department of Atmospheric Science Colorado State University Fort Collins, Colorado 80523	CDWA1A/02-1337 (FY-84)
	11. CONTRACT/GRANT NO.
	68-02-3731
12. SPONSORING AGENCY NAME AND ADDRESS	13. TYPE OF REPORT AND PERIOD COVERED
Environmental Sciences Research Laboratory-RTP, NC Office of Research and Development U.S. Environmental Protection Agency Research Triangle Park, North Carolina 27711	Final 9/30/81-3/30/83
	14. SPONSORING AGENCY CODE
	EPA/600/09

15. SUPPLEMENTARY NOTES

16. ABSTRACT

As part of the input for their regional-scale photochemical oxidant model of air pollution, known as the Regional Oxidant Model, the U.S. Environmental Protection Agency (EPA) requires statistical descriptions of total cloud amount, cumulus cloud amount, and cumulus cloud top height for certain regions and dates. These statistics are used to parameterize photochemical reactions, and to diagnose vertical transport of pollutants. The purpose of this work was to derive these statistics from digital satellite data.

The first stage of the work was to apply a human-computer interactive technique to satellite data to distinguish cumulus clouds from clouds of other types, and to produce the cloud amount statistics for cells within specified grids. Next, the interactive technique was applied to the infrared data to calculate the mean cloud top temperature for each cell. Those mean temperatures were then converted to heights by referring to objectively analyzed temperature versus height information derived from rawinsonde data. A frequency distribution of cumulus cloud top heights was also produced for some cases. The method was constrained by characteristics of the instrument systems employed and by certain atmospheric and cloud properties.

Information for users of the results is provided, including the dates, times and regions analyzed, output formats, and a discussion of special conditions within the output data.

17. KEY WORDS AND DOCUMENT ANALYSIS

a. DESCRIPTORS	b. IDENTIFIERS/OPEN ENDED TERMS	c. COSATI Field/Group

18. DISTRIBUTION STATEMENT	19. SECURITY CLASS *(This Report)*	21. NO. OF PAGES
RELEASE TO PUBLIC	UNCLASSIFIED	49
	20. SECURITY CLASS *(This page)*	22. PRICE
	UNCLASSIFIED	

EPA Form 2220-1 (Rev. 4-77) PREVIOUS EDITION IS OBSOLETE

NOTICE

This document has been reviewed in accordance with U.S. Environmental Protection Agency policy and approved for publication. Mention of trade names or commercial products does not constitute endorsement or recommendation for use.

ABSTRACT

As part of the input for their regional-scale photochemical oxidant model of air pollution, known as the Regional Oxidant Model, the U.S. Environmental Protection Agency (EPA) requires statistical descriptions of total cloud amount, cumulus cloud amount, and cumulus cloud top height for certain regions and dates. These statistics are used to parameterize photochemical reactions, and to diagnose vertical transport of pollutants. The purpose of this work was to derive these statistics from digital satellite data.

The first stage of the work was to apply a human-computer interactive technique to satellite data from the visible spectral channel and infrared window channel to distinguish cumulus clouds from clouds of other types, and to produce the cloud amount statistics for cells within specified grids. Next, the interactive technique was applied to the infrared data to calculate the mean cloud top temperature for each cell. Those mean temperatures were then converted to heights by referring to objectively analyzed temperature versus height information derived from rawinsonde data. A frequency distribution of cumulus cloud top heights was also produced for some cases.

The method was subject to several limitations. The recognition of cloud presence was constrained by the horizontal resolution of the visible sensor and the difficulty in detecting thin cirrus clouds. Cloud type identification was limited by occasional multilayered clouds, and the absence of sunlight at a few analysis times. Cumulus cloud top height determination was affected by long wave emission from atmospheric water vapor, the response time of the IR sensor, interference of multilayered clouds, and errors in the rawinsonde data. Cloud location was also affected by the satellite viewing angle. As a result of these constraints a cloud top height maximum error of 462 meters can be expected.

Information for users of the results is provided, including the dates, times, and regions analyzed, output formats, and a discussion of special conditions within the output data.

The successful completion of these tasks should allow the Regional Oxidant Model to be more accurate and complete. Recommended further work includes an intercomparison of results from other data platforms, and efforts to reduce the impact of cirrus clouds.

This report is submitted in fulfillment of Contract No. 68-02-3731 by Colorado State University under the sponsorship of the U.S. Environmental Protection Agency. This report covers the period September 30, 1981 to March 30, 1983, and work was completed as of March 31, 1983.

TABLE OF CONTENTS

Abstract. iii

List of Figures vi

List of Tables. vi

List of Acronyms and Symbols. vii

Acknowledgements. . . . . .

1. Introduction. 1

2. Technical Discussion. 2
   2.1 Generation of Cloud Statistics 2
   2.2 Limitations of the Method. 9
   2.3 Error Analysis 12
   2.4 Using the Results. 15

3. Conclusions and Recommendations 34

References. 35

Appendix. 36

LIST OF FIGURES

Number		Page
1	Example of cloud classification technique utilizing data from a) visible channel, and (b) IR channel to produce (c) a color-coded classification, where red (gray in black and white) shows cumulus cloud and yellow (white) shows cirrus.	3
2	Sample two-dimensional histogram of infrared versus visible brightness of different cloud types. . . .	6
3	Exaggerated depiction of apparent displacement of a cloud positioned a finite distance above the earth's surface.	13
4	Region covered by grid for Task 0. Western (W) and Eastern (E) sectors are shown.	16
5	Region covered by grid for Task 1.	18
6	Region covered by grid for Task 2.	20
7	Regions covered by grids for Task 3. (a) represents grid for August 7, 8, 1980, (b) is grid for August 9, 10, 11, 1980. Sector identifiers are shown . .	28
8	Region covered by grid for Task 4. Western (W) and Eastern sectors are shown	30

LIST OF TABLES

1	Output for Task 0.	15
2	Output for Task 1.	19
3	Output for Task 2 and Task 3	21
4	Output for Task 4.	31

List of Acronyms and Symbols

Acronyms

CSU	Colorado State University
EPA	Environmental Protection Agency
GOES	Geostationary Operational Environmental Satellite
IRIS	Interactive Research Imaging System
LIDAR	Light Detection and Ranging
NASA	National Aeronautics and Space Administration
NEROS	Northeast Regional Oxidant Study
NOAA/EDIS	National Oceanic and Atmospheric Administration/ Environmental Data Information Service

Symbols

A_c	Area covered by aperture of satellite radiometer
B	The Planck function
C_D	Digital Satellite data value
C_1, C_2	Constants in the Planck's function
f	Satellite radiometer calibration function
g	Digitizing function for satellite data
N	Fractional cloud amount within an IR pixel
$N_{r\lambda}$	Spectral irradiance received at satellite radiometer
p	Atmospheric pressure
P_r	Electromagnetic power
T	Temperature
V_o	Voltage produced by satellite radiometer
a	Aperture of satellite radiometer
ε_s	Emittance of a cloud or ground surface
Γ	Atmospheric lapse rate
λ	Electromagnetic wavelength
τ	Atmospheric transmittance

ACKNOWLEDGEMENTS

The authors would like to express their gratitude to the U.S. Department of Interior, Bureau of Reclamation in Denver, Colorado for supplying the rawinsonde data used in this study. Mrs. Judith Bonds was particularly helpful in that matter. We also wish to thank the National Oceanic and Atmospheric Administration/Environmental Data Information Service and personnel at the GOES Data Archive, University of Wisconsin for providing the digital satellite data and answering various questions regarding those data. Finally, Ms. Robin Wilson's typing of the manuscript and Mrs. Judy Sorbie's drafting of figures were greatly appreciated.

SECTION 1
INTRODUCTION

One of the ways in which the U.S. Environmental Protection Agency (EPA) seeks to fulfill its duty to promote a healthy environment is by simulating the production, transport, and fate of atmospheric pollutants with numerical models. A comprehensive regional ozone model of this type has been developed at the EPA [Lamb (1983)]. It is called the Regional Oxidant Model. Among the processes simulated by the model are the formation of oxidant pollutants by photochemical reactions and the transport of pollutants away from their sources. Successful parameterization of these effects requires many types of special data as input. Photochemical reactions occur in the presence of sunlight, and their parameterization requires knowledge of the cloud cover, among other things. Vertical transport of pollutants is accomplished by convection, and horizontal transport is affected by the vertical transport in that the horizontal wind velocity varies with altitude. Cumulus clouds provide an indication of the extent and intensity of vertical transport within the atmosphere by virtue of their manifestation of convection.

The purpose of the work reported here was to supply the EPA with the special data needed for modelling the processes mentioned above. The cases analyzed occurred during the EPA's Northeast Regional Oxidant Study (NEROS II) and during the National Aeronautics and Space Administration's (NASA) 1981 Summer Experiment. Those field programs also supplied other types of special data which will be incorporated with the satellite-derived data as input to the model. Digital satellite data transmitted from the Geostationary Operational Environmental Satellite (GOES) were analyzed with the help of Colorado State University's (CSU) Interactive Research Imaging System (IRIS) in order to generate the required diagnoses of total cloud amount, cumulus cloud amount, and cumulus cloud top height. Synoptic rawinsonde data also were used in translating cloud top temperatures to cloud top heights. Digital satellite data were essential to the success of the study because they provided uniform spatial coverage (unlike surface station data) and because they were readily processed by human-computer interactive techniques. These interactive techniques were faster than manual analyses of hard copy satellite images would have been, and they produced more precise cloud top height determinations due to the availability of a wide range of infrared digital counts, rather than the narrow range of gray-shades seen on hard copy images. The IRIS was equally important in producing the quantitative cloud field statistics supplied to EPA in that it made possible the manipulation of the digital data. A description of the IRIS is contained in Appendix A.

SECTION 2
TECHNICAL DISCUSSION

2.1 GENERATION OF CLOUD STATISTICS

The cloud field statistics produced for the EPA were derived by a two step process. The first step involved displaying the digital satellite data with the IRIS and generating values for total cloud amount, cumulus cloud amount, and cumulus cloud top temperature. The second step was to convert the cumulus cloud top temperature values to cloud top height values by referring to rawinsonde-derived vertical profiles of atmospheric temperature. Details of these procedures are contained in the following subsections.

2.1.1 Satellite Data Analysis

GOES digital satellite data in the visible channel and infrared window (transparent to the earth's surface where cloud free) channel were obtained by CSU from the National Oceanic and Atmospheric Administration's Environmental Data Information Service (NOAA/EDIS). The GOES data archive is maintained for NOAA/EDIS by the Space Science and Engineering Center at the University of Wisconsin. The visible and infrared data were preprocessed within the IRIS to decode the format and then displayed in image form on a video monitor. Sample images are shown in Figure 1. The horizontal resolution of the visible data was 0.92 km at the subsatellite point (75°W, 0°N), whereas the resolution of the IR data was 4 km by 8 km. The resolution of the satellite data is defined by the area projected by the satellite radiometer field of view upon the earth's surface. That resolution specifies the size of the smallest cloud which can be observed by the satellite. These resolution values were slightly larger at the latitudes and longitudes of interest for this study. For instance at 36°N, 76°W the resolution of the visible channel data was 0.96 km by 1.22 km, whereas at 45°N, 86°W the resolution was 1.14 km by 1.44 km.

The satellite-derived cloud statistics were output in gridded form so that they can be easily read into EPA's pollution model. The values of total cloud amount and cumulus cloud amount apply to individual grid cells, whereas the cloud top heights are mean values for each cell. In general, each output grid cell had dimensions of 1/6 degree latitude by 1/4 degree longitude. Specific regions covered by the grids used for the various cases, along with details on grid cell resolution, are described in section 2.4. It is worth noting that each grid was made rectangular with respect to lines of latitude and longitude in order to facilitate participation of the computer in generating statistics.

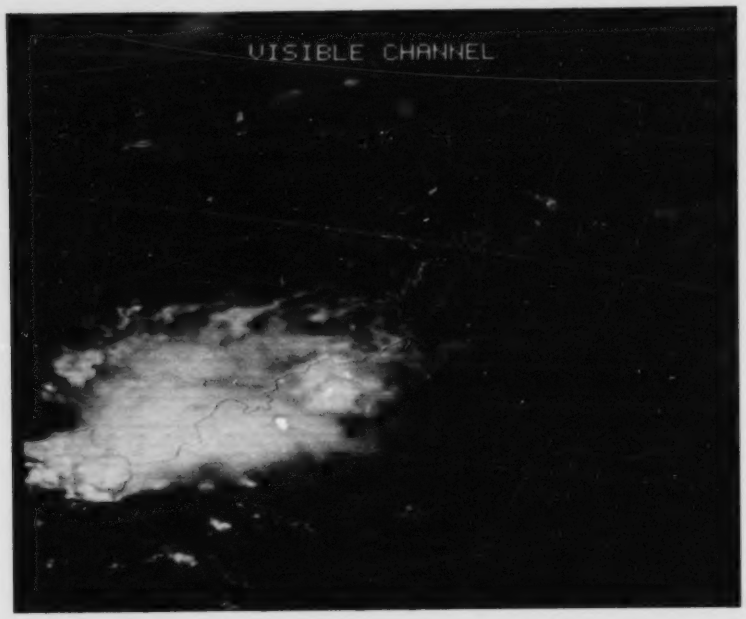

(a)

B & W photos not available for pg 3 + 4

(b)

Figure 1. Example of cloud classification technique utilizing data from (a) visible channel, and (b) IR channel to produce (c) a color-coded classification, where red (grey in black and white) shows cumulus cloud and yellow (white) shows cirrus.

(c)

Figure 1. Continued

Navigation of the satellite data was a routine, but important, part of the analysis. Navigation is the creation of a mapping between points in the coordinate system of the satellite image and geographic points on the earth. Precise navigation of the data ensured that the geographic location of each grid cell was known. The accuracy of the navigation of each image was checked by overlaying maps of coastlines, lakes, and reservoirs based upon the navigation calculations. Any discrepancies between those plots and visibly identified landmarks indicated a need to revise the navigation. Finally, care was taken to make sure that cloud features within the visible and infrared images were aligned.

Once preliminary tasks such as image display and navigation were performed for each visible-IR image pair, which corresponded to a particular date and time, the central task of applying the interactive technique developed at CSU to calculate the statistics was begun. In order to streamline the technique, special computer software was written and installed in the IRIS.

The interactive technique was bispectral in nature. Simultaneous analyses of the coincident visible and IR images allowed CSU scientists to distinguish cumulus clouds from clouds of other types. The physical basis for this method is illustrated in Figure 2. It is founded on the observational evidence that different cloud types usually fall on different parts of a two-dimensional histogram of visible brightness versus infrared brightness [ESA (1980), Desbois et al. (1982)]. For instance, cirrus clouds appear colder than the underlying surface, but they generally are slightly darker in visible wavelengths than deep cumuli.

Thresholds for the visible and infrared channels were interactively selected by color-coding their effects on the cloud classification and displaying the result on the IRIS. (See Figure 1 for an example.) Once finalized, these thresholds allowed the computer to separately count the number of picture elements (pixels) which corresponded to cumulus clouds and other types of clouds. The IRIS then compiled these figures into statistics of total cloud amount and cumulus cloud amount for each grid cell.

Calculation of the mean cloud top temperature, from which cloud top heights were derived subsequently, depended largely upon satellite data from the infrared spectral channel. That channel is centered on a wavelength of 11.5 μm, and is sensitive to thermally emitted radiation. The translation of the digital value C_D into the apparent (or brightness) temperature of a cloud or the earth's surface was accomplished in the following manner:

$$C_D = g(V_o) \tag{1}$$

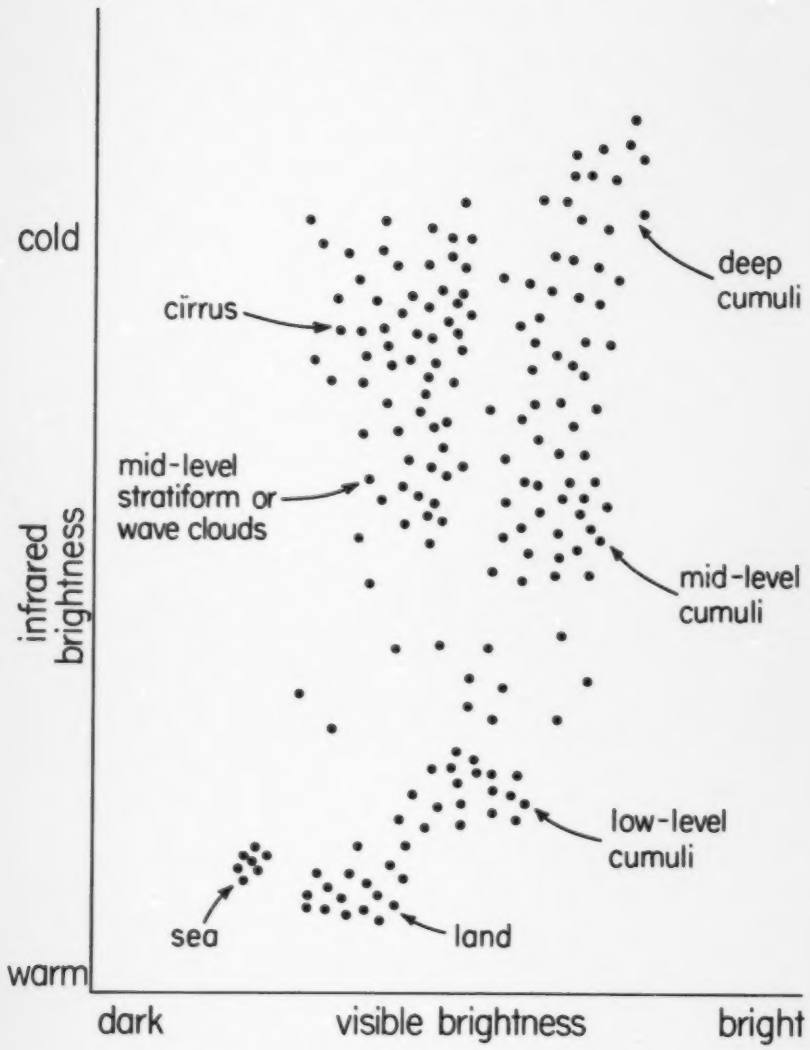

Figure 2. Sample two-dimensional histogram of infrared versus visible brightness of different cloud types.

where g is a specified digitizing function, and V_o is the voltage produced by the satellite-mounted radiometer. In turn,

$$V_o = f(P_r) \tag{2}$$

where f is a known calibration function, and P_r is the electromagnetic power received at the radiometer. Now, the spectral irradiance received at the radiometer ($N_{r\lambda}$) is

$$N_{r\lambda} = \frac{4P_r}{A_c \pi \alpha^2} \tag{3}$$

where α is the aperture of the radiometer, and A_c is the area covered by that aperture. $N_{r\lambda}$ is related to temperature by

$$N_{r\lambda} = \varepsilon_s B(T_s)\tau(p_o) - \int_o^{p_o} B(T(p)) \frac{d\tau}{dp} dp \tag{4}$$

where ε_s is the emittance of a surface (earth or cloud), τ is the atmospheric transmittance, p is pressure, T is temperature, and B is the Planck function. The first term on the right hand side of Equation 4 represents the radiant exitance of a cloud or the earth's surface, whereas the second term gives the exitance generated by the atmosphere. Since the spectral channel in question is a window channel, that second term is small, and $\tau(p_o) \simeq 1$. Finally, ε_s is assumed equal to one for cumulus clouds, which are optically thick, and Planck's law yields

$$B(Ts) = \frac{c_1 \lambda^{-5}}{e^{c_2/\lambda T_s} - 1} \tag{5}$$

where λ is the wavelength. In practice, these theoretical considerations were condensed into a lookup table, which converted digital values to equivalent brightness temperatures.

An important consideration regarding the rather large area covered by a single infrared pixel was taken into account in the course of this work. Because many cumulus clouds were smaller than the projection of

the infrared sensor's field of view on the earth, the satellite-observed temperature for a spot including such a cloud was contaminated by the apparent background surface temperature. This effect was corrected by computing the cloud top temperature as a function of the observed temperature, the background surface temperature, and the percent cloud cover. The weighted brightness temperature of a single observed IR pixel is given by

$$T_o = N\,T_{CT} + (1 - N)T_B \tag{6}$$

where T_o is the temperature of the observed pixel, T_{CT} is the cloud top temperature, T_B is the background surface temperature, and N is the fractional cloud amount within the IR pixel. This equation was inverted to give the cloud top temperature:

$$T_{CT} = \frac{T_o - (1 - N)T_B}{N} \tag{7}$$

In applying Equation 7, T_B was estimated from the minimum T_o within the grid cell being processed, and N was calculated from the higher resolution visible channel. The method described above is analogous to that of Reynolds and Vonder Haar (1977).

A problem similar to that of a partly filled sensor field of view occurred when multilayer clouds were present within the field of view. However, that problem is more difficult to treat because multilayer clouds are harder to detect with data from just two spectral channels than is infrared channel contamination by the surface thermal emission.

For some of the cases analyzed, a frequency distribution of cloud top heights was required. Values of T_{CT} for individual IR pixels were saved for those cases, which are defined in Section 2.4. Otherwise, a mean T_{CT} was all that was computed for each grid cell.

2.1.2 Calculation of Cloud Top Heights

The final task that was performed in order to produce the results needed by the EPA was the conversion of the satellite-derived cumulus cloud top temperatures into cloud top heights above mean sea level. The information on the vertical temperature structure of the atmosphere required for this task was derived from standard synoptic rawinsonde sounding data, which were obtained on microfiche from the United States

Department of Interior, Bureau of Reclamation, in Denver, Colorado. These data were punched on computer cards at CSU for input to the computer. Rawinsonde data were utilized from stations surrounding and within the area of interest for each case. In addition, soundings from times encompassing the times of interest for this study were analyzed. For instance, soundings from 1200 GMT and 0000 GMT were used to diagnose the atmospheric vertical temperature structure at 1600 GMT. These procedures were followed in recognition of the fact that the temperature structure varies with space and time.

An objective analysis technique was utilized to incorporate the rawinsonde data into the study. The reasons for this approach were that it allowed objective horizontal interpolation of the vertical temperature structure from the coarse scale of the sounding network down to the rather fine scale of the grids used in this work, and that it allowed the rapid processing of large quantities of rawinsonde data. The first stage of the objective analysis involved finding the temperature at certain fixed height levels within the atmosphere for each rawinsonde station. This was accomplished by performing a linear interpolation in the vertical between the levels available from each sounding. The fixed levels used were at 100 m, 500 m, 1000 m, 2000 m, 3000 m, and so on to 17000 m. At this point in the process, several data points from the stations were available at each fixed level. Next, the data points at each level were input to a Barnes objective analysis [Barnes (1973), (1964)] computer program, and a gridded field of temperatures was produced for each level. The result was a three-dimensional grid of temperatures with the same horizontal resolution as that of the satellite-derived statistics. As mentioned above, such temperature-height fields were calculated for times surrounding the times under study.

The actual conversion of a cloud top temperature to a cloud top height was initiated by vertically interpolating the mean cloud top temperature for a grid cell between temperatures at the fixed levels to find a corresponding height above mean sea level within the atmosphere. Assuming that the temperature of the cloud top was the same as that observed by the rawinsonde at that level, a cloud top height was assigned by the computer. If a frequency distribution of cloud top heights was required, this process was repeated several times. In cases where a particular temperature occurred at two different levels in the atmosphere, the cloud top height was assigned at the lower level under the assumption that further convective growth was limited by the implied temperature inversion.

2.2 LIMITATIONS OF THE METHOD

Although the technical approach discussed above was designed to avoid many of the inaccuracies and special conditions associated with calculating the required cloud field statistics from digital satellite data, certain constraints were present which limited CSU's ability to provide EPA with perfectly complete and accurate statistics. A discussion of these limitations as they apply to the various subtasks follows.

2.2.1 Cloud/No-Cloud Identification

The identification of regions with cloud cover and regions with no cloud depended on the ability of the scientist involved to select a brightness threshold for the visible channel that delineated those areas. The first constraint on this process was related to the size of the geographic area seen within a single field of view of the satellite's visible sensor. In general, the smallest cloud feature resolved by the visible sensor was approximately 1.5 km^2 in area at the latitudes and longitudes studied. Small clouds of the type cumulus humilis (fair weather cumulus) usually are smaller than this limit, making their detection with GOES data difficult to impossible. Very high resolution data from polar orbitting satellites would be required to identify those small clouds. Such data generally were not available at the times and places needed for this study. However, the impact of this limitation on EPA's model is somewhat reduced by the fact that cumulus humilis clouds are quite short-lived, and that they do not represent significant vertical transport beyond dry mixing processes, which would not be diagnosed by these methods anyway.

A second constraint on the cloud amount analysis was the difficulty with identifying optically thin cirrus clouds. Cirrus clouds sometimes were so thin that they did not reflect an amount of visible radiation that was distinguishable from that reflected by the surface. Identification from the infrared window channel also was difficult. Thin cirrus clouds were easier to recognize over the ocean than over land because the sea appeared visibly darker. For consistency, very thin cirrus was uniformly ignored as cloud cover, regardless of the background.

2.2.2 Cloud Type Identification

A second class of limitations affected CSU's ability to identify cumulus clouds and distinguish them from other types of clouds. Probably the most common difficulty in this class was the presence of multilayer clouds. For instance, there is no doubt that cirriform cloudiness generated from cumulonimbus anvils often concealed new cumulus growth beneath it. The only readily available source of information on the presence of such concealed cumuli is surface station data. Cloud cover reports from surface data present certain problems, though, including the lack of uniform spatial coverage, the lack of precision in specifying fractional cloud coverage and cloud top height, and the difficulty that would be encountered trying to incorporate those data into the interactive computing procedures used at CSU. For these reasons, no attempt was made to incorporate surface station cloud reports into this study.

A second limitation that sporadically affected cloud type identification was the requirement to calculate cloud statistics for a few times after the sun had set at the location of interest. This fact rendered the visible data useless for all times after 2000 EDT. After 2000 EDT all of the statistics were derived from infrared data alone.

It is believed that this change did not seriously affect the analysis of total cloud cover. However, the analyses of cumulus cloud cover and cumulus cloud top height depended on the bispectral technique, and these results were less accurate at the times in question. In most cases the cumulus cloud amount and cloud top height were underestimated from the IR data only.

2.2.3 Cloud Top Height Determination

Another set of contraints impacted the determination of cloud top heights at CSU. The first constraint was related to thermal emission by atmospheric water vapor. Water vapor does have a small emittance in the 11 μm IR channel used in this study, and the absorption and subsequent radiation by water vapor between the target (cloud or ground) and the radiometer can cause the target to appear colder than it really is. The impact of this process on a satellite-derived surface temperature has a magnitude of approximately 4°C [Kivel (1978)]. However, the effect of water vapor emission on the cloud top temperatures derived in this study was negligible due to the fact that a great majority of atmospheric water vapor is in the subcloud layer. Also, the values of T_B used in Equation 7 accounted for the effect by using satellite-derived background temperatures, with water vapor emission included, rather than surface-based temperature measurements.

A second influence on the calculated cloud top temperatures was the response time of the IR sensor. Normally, that sensor does not respond immediately to a rapid change in temperature as it scans across a scene. Therefore, the temperature near the edge of a tall, cold cumulus cloud was likely to be overestimated. The magnitude of this error ranges from 1 to 5°C, depending on the actual cloud top and background temperatures and the configuration of clouds [Adler and Markus (1982)].

Another problem, mentioned above, was the possibility that the temperature of a cloud top might not be the same as that measured by rawinsonde for a particular height within the atmosphere. Potential causes of this effect were differential thermal radiation between cloud and environment, and cooling of cloud parcels at moist adiabatic rates. However, it has been found [Pitts *et al.* (1975)] that this error is rather small in most cases.

A limitation that was related to the occasional presence of multilayer clouds sometimes created difficulties in calculating cumulus cloud top temperatures. Due to their large size, it was possible for infrared pixels to contain cumulus clouds and clouds of another type. Such pixels would have yielded cloud top temperatures that were not entirely representative of cumulus clouds. In order to minimize this problem, a cloud top temperature was not calculated from any IR pixel for which the total cloud cover was composed of less than 70 percent cumulus cloud.

The final sources of error in deriving the cloud top height were related to the rawinsonde data used to translate cloud top temperatures.

There were a few times for which rawinsonde data were not available from the Bureau of Reclamation. When data were not available, the conversion of temperatures to heights was accomplished using rawinsonde data from the single nearest time, rather than from the observation times surrounding the analysis time, as described in section 2.1. Secondly, all of the rawinsonde data had a much lower horizontal resolution than the resolution of the required temperature-height analyses. The horizontal resolution of the synoptic rawinsonde network ranged from 225 to 450 km, whereas the resolution of the temperature-height analyses was approximately 20 km. The Barnes objective analysis scheme interpolated the rawinsonde data down to the required horizontal scale. However, the temperature-height analyses cannot be expected to reproduce all of the mesoscale variations that, no doubt, were present.

2.2.4 Cloud Location

A constraint that affected all of the cloud statistics produced for the EPA was the misrepresentation of cloud locations due to the viewing angle between the satellite and the clouds. This phenomenon is illustrated in Figure 3. It results from the fact that a cloud top which is significantly above the earth's surface appears displaced away from the satellite along the line of sight. Of course, the effect is greater for deep clouds than for shallow ones. The impact on the cloud statistics was limited to erroneous placement of clouds near the edge of one grid cell into a neighboring grid cell. Although the magnitude of the error in cloud amount determinations caused by this phenomenon was a function of the cloud pattern, it probably was limited to about five percent in most cases.

2.3 ERROR ANALYSIS

Although many constraints on the accuracy of the calculated cloud field statistics have been discussed, a quantitative assessment of their combined impact on the statistics remains to be done. Such a quantitative evaluation is rather difficult to perform for the fractional coverage of total cloud and cumulus cloud results, though, because the limitations on these tasks could cause errors ranging from 0 to 100 percent. For instance, a field of cumulus humilis clouds sometimes could be entirely invisible to the visible channel sensor. Similarly, developing cumuli occasionally might be completely concealed by a large anvil from a nearby cumulonimbus cloud. For these reasons a quantitative assessment of those two parameters will not be attempted here. However, large errors in those quantities are believed to be infrequent.

It is possible to evaluate the error in cloud top height calculations. Since most of the sources of error in this quantity resulted from errors in the determination of mean cumulus cloud top temperature, the error analysis will be performed in terms of temperature, and then converted to an equivalent error in height at the

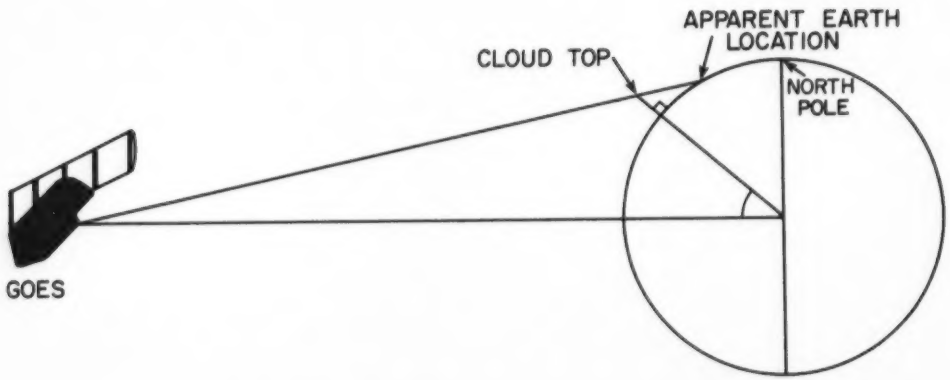

Figure 3. Exaggerated depiction of apparent displacement of a cloud positioned a finite distance above the earth's surface.

end. The maximum total error is defined as the sum of the absolute values of the contributing errors:

$$\Delta T_{max} = \sum_{i=1}^{n} |\Delta T_i| \tag{8}$$

The following values of the ΔT_i's are deemed representative, based upon the previous discussions:

ΔT_{Equil}	(difference between rawinsonde and cloud top temperature at some level)	$= 0.5^{o}C$
ΔT_{WV}	(H_2O vapor emission)	$= 0.5^{o}C$
ΔT_{Resp}	(IR sensor response time)	$= 2.0^{o}C$
ΔT_{HR}	(rawinsonde data horizontal resolution)	$= 1.0^{o}C$
ΔT_{VI}	(vertical interpolation of cloud top temperature)	$= 1.0^{o}$

Therefore,

$$\Delta T_{max} = 5.0^{o}C$$

under normal conditions. Now, the average lapse rate (Γ) of the U.S. Standard Atmosphere is $6.5^{o}C/km$. Applying this lapse rate to ΔT_{max} yields

$$\Delta H_{max} = \Delta T_{max}/\Gamma = 0.77 \text{ km}$$

$$= 770 \text{ m} = 2526 \text{ ft.}$$

In most cases the actual error was smaller due to offsetting individual errors. In almost all cases, ΔT_{Equil} and ΔT_{WV} caused an underestimate of cloud top temperature, whereas ΔT_{Resp} caused an overestimate. If the appropriate signs are given to those terms, the resulting ΔT is $3^{o}C$, which corresponds to a height error of 462 meters (1514 feet).

Another potential error has not been included in the above analysis due to its sporadic nature. That error was the contamination of cumulus cloud top temperatures by cirrus clouds that were too thin to be detected in either the visible or infrared channels. Although not detectable, thin cirrus could cool the observed cloud top temperature by

as much as an estimated $5^{o}C$, compared to the true temperature. A ΔT of this magnitude would cause a 770 meter cloud top height error by itself. Unfortunately, the data needed for a complete evaluation of this problem do not currently exist.

2.4 USING THE RESULTS

This section is intended to serve as a users' guide to the cloud field statistics generated at CSU. The formats of the output data; the dates, times, and regions analyzed; and any special conditions or problems relating to the results will be discussed. The discussions are logically organized by cases that utilized the same output grid. The organization also corresponds to that used in specifying tasks within the contract, where Task 0 corresponds to Exhibit A of the contract, Task 1 corresponds to Exhibit A-1 of the contract, Task 2 to Exhibit A-2, and so on. The regions covered by the output grids were chosen to correspond to the areas studied under EPA's NEROS II (Tasks 0 through 3) and NASA's 1981 Summer Experiment (Task 4).

2.4.1 Task 0

Output Specifications--

The output for Task 0 resides on Tape 1. The contents of that tape are shown in Table 1, along with the dates, times, and regions analyzed. Because of the size of the gridded region analyzed, the output data were provided for an eastern and a western sector. These sectors are shown in Figure 4.

Table 1
Output for Task 0

Tape #	File#	Date/Hour (EDT)	Sector
1	1	8/14/80, 0900	east
1	2	8/14/80, 0900	west
1	3	8/14/80, 1200	east
1	4	8/14/80, 1200	west
1	5	8/14/80, 1500	east
1	6	8/14/80, 1500	west
1	7	8/14/80, 1830	east
1	8	8/14/80, 1830	west

as much as an estimated $5^{o}C$, compared to the true temperature. A ΔT of this magnitude would cause a 770 meter cloud top height error by itself. Unfortunately, the data needed for a complete evaluation of this problem do not currently exist.

2.4 USING THE RESULTS

This section is intended to serve as a users' guide to the cloud field statistics generated at CSU. The formats of the output data; the dates, times, and regions analyzed; and any special conditions or problems relating to the results will be discussed. The discussions are logically organized by cases that utilized the same output grid. The organization also corresponds to that used in specifying tasks within the contract, where Task 0 corresponds to Exhibit A of the contract, Task 1 corresponds to Exhibit A-1 of the contract, Task 2 to Exhibit A-2, and so on. The regions covered by the output grids were chosen to correspond to the areas studied under EPA's NEROS II (Tasks 0 through 3) and NASA's 1981 Summer Experiment (Task 4).

2.4.1 Task 0

Output Specifications--

The output for Task 0 resides on Tape 1. The contents of that tape are shown in Table 1, along with the dates, times, and regions analyzed. Because of the size of the gridded region analyzed, the output data were provided for an eastern and a western sector. These sectors are shown in Figure 4.

Table 1
Output for Task 0

Tape #	File#	Date/Hour (EDT)	Sector
1	1	8/14/80, 0900	east
1	2	8/14/80, 0900	west
1	3	8/14/80, 1200	east
1	4	8/14/80, 1200	west
1	5	8/14/80, 1500	east
1	6	8/14/80, 1500	west
1	7	8/14/80, 1830	east
1	8	8/14/80, 1830	west

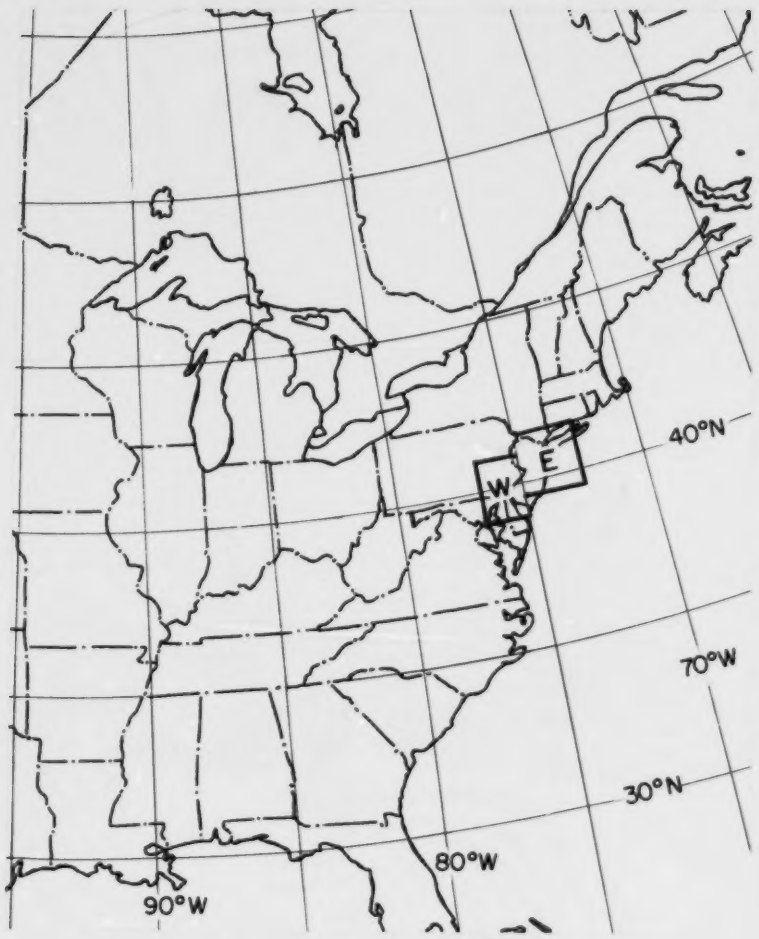

Figure 4. Region covered by grid for Task 0. Western (W) and Eastern (E) sectors are shown.

Format--

The data were written in ASCII at 1600 bpi. Each record contains the output for one grid at one time. The format of each record is as follows (in FORTRAN notation):

(3I2, I5, 2F10.3, 2F6.3, F5.0),

where the first three words denote the day, month, and year, respectively, the next word represents the time (EDT), the next two words give the latitude (^{o}N) and longitude (^{o}W) of the lower left corner of the grid cell, the next two words represent the fractional coverage of all clouds and cumulus clouds, respectively, and the last word denotes the average cumulus cloud top height (hundreds of feet). A cumulus cloud top height of -999 signifies that no cumuli were present, or that pixels with cumuli also were contaminated by other cloud types.

Special Conditions--

The only problem that affected the performance of Task 0 was the inability of NOAA/EDIS to provide satellite data to CSU for 1800 EDT on August 14, 1980. Rather, data from 1830 EDT were received and analyzed.

2.4.2 Task 1

Output Specifications--

The output for Task 1 resides on Tape 3. The contents of this tape, along with the dates, times, and regions analyzed are shown in Table 2. The single sector covered by the grid used for Task 1 is outlined in Figure 5. For this task only, the size of each grid cell was 1/12 degree latitude by 1/8 degree longitude. Note that the last two files on Tape 3 are from Task 4, the output for which will be discussed in section 2.4.5.

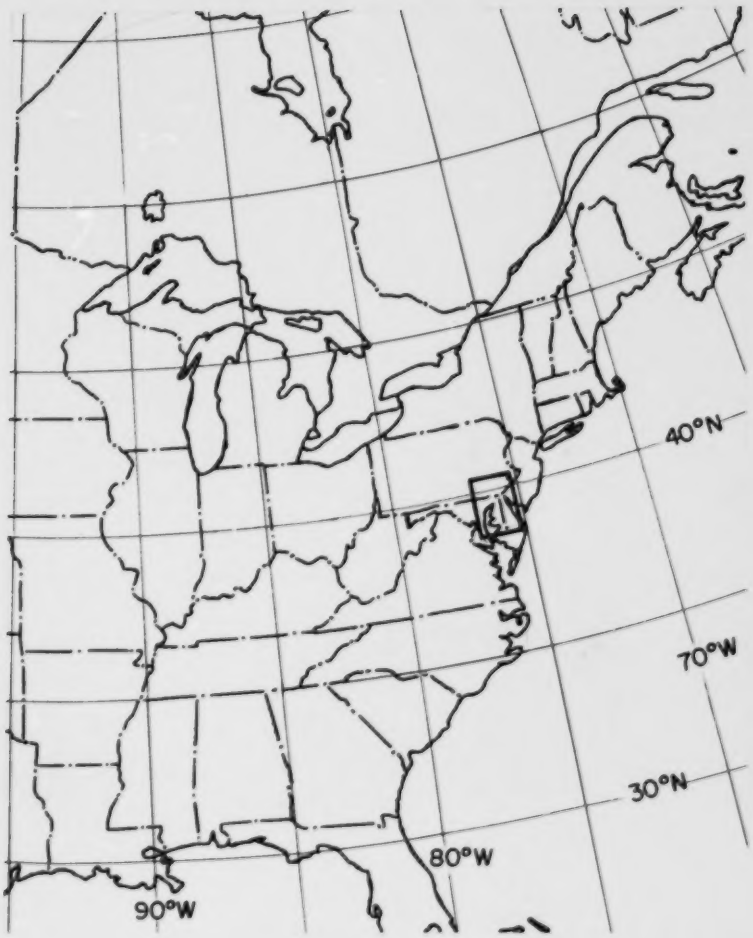

Figure 5. Region covered by grid for Task 1.

Table 2
Output for Task 1

Tape #	File #	Date/Hour (EDT)	Sector
3	1	7/25/80, 0900	Entire
3	2	7/25/80, 1200	Entire
3	3	7/25/80, 1500	Entire
3	4	7/25/80, 1800	Entire
3	5	8/2/80, 0900	Entire
3	6	8/2/80, 1200	Entire
3	7	8/2/80, 1500	Entire
3	8	8/2/80, 1800	Entire
3	9	8/5/80, 0900	Entire
3	10	8/5/80, 1500	Entire
3	11	8/5/80, 1800	Entire
3	12	7/28/81, 2300*	East
3	13	7/28/81, 2300*	West

*derived from IR data only.

Format—

The format of the output for Task 1 is the same as for Task 0. Refer to section 2.4.5 for the format of the last two files.

Special Conditions—

The digital satellite data sent to CSU by NOAA/EDIS for 1200 EDT on August 5, 1980 were of extremely poor quality due to severe noise within many of the data records. No cloud field statistics were produced by CSU for that time.

2.4.3 Task 2

Output Specifications—

The output for Task 2 is on files 1 through 43 of Tape 4. Table 3 shows the dates, times, and regions analyzed. The sector used for Task 2 is outlined in Figure 6. A frequency distribution of cumulus cloud top heights is provided for each grid cell in Task 2, in addition to a mean cumulus cloud top height for the entire cell. The frequency distribution is given in terms of the number of pixels of satellite data corresponding to each of 40 height classes. Each class is 500 feet deep. The first class corresponds to the 500 to 999 foot layer, the second class to the 1000 to 1499 foot layer, and so on. The last class contains a count of pixels exceeding 19999 feet.

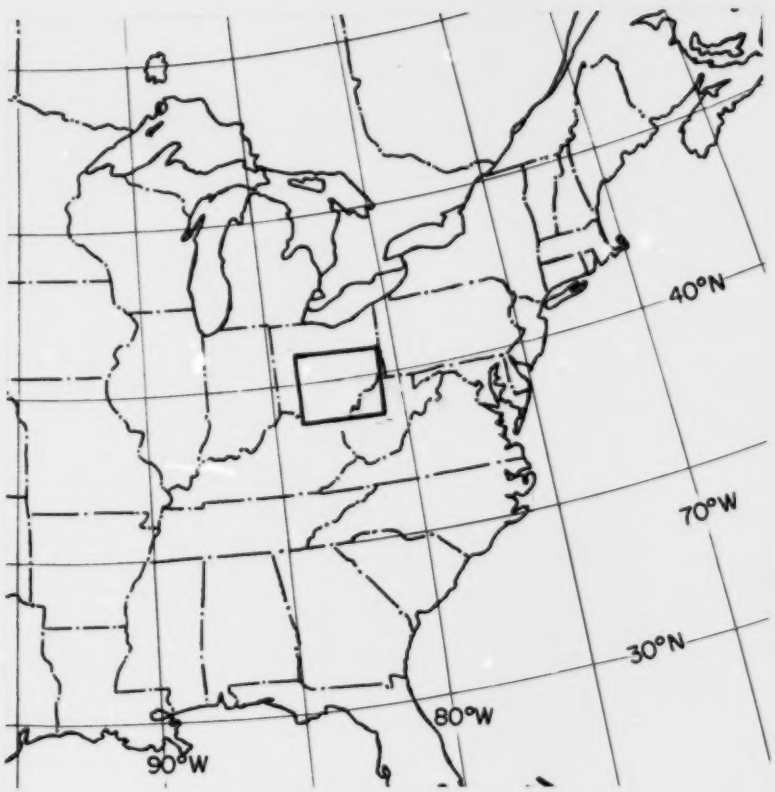

Figure 6. Region covered by grid for Task 2.

Table 3
Output for Task 2 and Task 3

Tape #	File #	Date/Hour (EDT)		Sector
4	1	7/30/80	1000	Entire
	2		1200	Entire
	3		1400	Entire
	4		1800	Entire
	5	8/4/80	1200	Entire
	6		1400	Entire
	7		1500	Entire
	8		1600	Entire
	9		1800	Entire
	10		2000	Entire
	11	8/5/80	1400	Entire
	12	8/8/80	1200	Entire
	13		1300	Entire
	14		1400	Entire
	15	8/12/80	1300	Entire
	16		1500	Entire
	17		1600	Entire
	18		1700	Entire
	19		1900	Entire
	20	8/13/80	1100*	Entire
	21		1300	Entire
	22		1400	Entire
	23		1500	Entire
	24		1600	Entire
	25		1700	Entire
	26		1900	Entire
	27	8/16/80	1100	Entire
	28		1200	Entire
	29		1300	Entire
	30		1400	Entire
	31	8/22/80	1500	Entire
	32		1600	Entire
	33		1700	Entire
	34	8/23/80	1500	Entire
	35		1600	Entire
	36		1700	Entire
	37	8/24/80	1400	Entire
	38		1500	Entire
	39		1600	Entire
	40	8/25/80	1300	Entire
	41		1400	Entire
	42		1500	Entire
	43		1600	Entire
	44	8/9/80	1300	1N
	45		1300	1S
	46		1300	2N
	47		1300	2S

*misprepresented as 0900 EDT within output records.

Tape #	File #	Date/Hour (EDT)		Sector
4	48	8/9/80	1300	3N
	49		1300	3S
	50		1300	4N
	51		1300	4S
	52		1600	1N
	53		1600	1S
	54		1600	2N
	55		1600	2S
	56		1600	3N
	57		1600	3S
	58		1600	4N
	59		1600	4S
	60		1900	1N
	61		1900	1S
	62		1900	2N
	63		1900	2S
	64		1900	3N
	65		1900	3S
	66		1900	4N
	67		1900	4S
		END OF VOLUME		
5	1	8/9/80	2200*	1N
	2		2200*	1S
	3		2200*	2N
	4		2200*	2S
	5		2200*	3N
	6		2200*	3S
	7		2200*	4N
	8		2200*	4S
	9	8/10/80	1300	West
	10		1300	West Central
	11		1300	East Central
	12		1300	East
	13		1600	West
	14		1600	West Central
	15		1600	East Central
	16		1600	East
	17		1900	1N
	18		1900	1S
	19		1900	2N
	20		1900	2S
	21		1900	3N
	22		1900	3S
	23		1900	4N
	24		1900	4S

*from IR data only

Tape #	File #	Date/Hour (EDT)		Sector
5	25	8/10/80	2200*	1N
	26		2200*	1S
	27		2200*	2N
	28		2200*	2S
	29		2200*	3N
	30		2200*	3S
	31		2200*	4N
	32		2200*	4S
	33	8/11/80	1300	1N
	34		1300	1S
	35		1300	2N
	36		1300	2S
	37		1300	3N
	38		1300	3S
	39		1300	4N
	40		1300	4S
	41		1600	1N
	42		1600	1S
	43		1600	2N
	44		1600	2S
	45		1600	3N
	46		1600	3S
	47		1600	4S
	48		1600	4N
	END OF VOLUME			
6	1	8/11/80	1900	1N
	2		1900	1S
	3		1900	2N
	4		1900	2S
	5		1900	3N
	6		1900	3S
	7		1900	4N
	8		1900	4S
	9		2200*	1N
	10		2200*	1S
	11		2200*	2N
	12		2200*	2S
	13		2200*	3N
	14		2200*	3S
	15		2200*	4N
	16		2200*	4S
	17	8/7/80	1300	1N
	18		1300	1S
	19		1300	2N
	20		1300	2S
	21		1300	3N
	22		1300	3S
	23		1300	4S

*from IR data only

Tape #	File #	Date/Hour (EDT)		Sector
6	24	8/7/80	1300	5N
	25		1300	5S
	26		1600	1N
	27		1600	1S
	28		1600	2N
	29		1600	2S
	30		1600	3N
	31		1600	3S
	32		1600	4N
	33		1600	4S
	34		1600	5N
	35		1600	5S
	36		1900	1N
	37		1900	1S
	38		1900	2N
	39		1900	2S
	40		1900	3N
	41		1900	3S
	42		1900	4N
	43		1900	4S
	44		1900	5N
	45		1900	5S
	46		1300	4N
	47		2200*	1N
	48		2200*	1S
	49		2200*	2N
	50		2200*	2S
	51		2200*	3N
	52		2200*	3S
	53		2200*	4N
	54		2200*	4S
	END OF VOLUME			
7	1	8/8/80	1300	1N
	2		1300	1S
	3		1300	2N
	4		1300	2S
	5		1300	3N
	6		1300	3S
	7		1300	4N
	8		1300	4S
	9		1300	5N
	10		1300	5S
	11		1900	1N
	12		1900	1S
	13		1900	2N
	14		1900	2S
	15		1900	3N
	16		1900	3S
	17		1900	4N

*from IR data only

Tape #	File #	Date/Hour (EDT)		Sector
7	18	8/8/80	1900	4S
	19		1900	5N
	20		1900	5S
	21		2200*	1N
	22		2200*	2N
	23		2200*	2S
	24		2200*	3N
	25		2200*	3S
	26		2200*	4N
	27		2200*	4S
	END OF VOLUME			

*from IR data only

Format--

The data were written in ASCII at 1600 bpi. The output for a single grid cell is contained on two consecutive records. The format of the first record is as follows (in FORTRAN notation):

(3I2, I5, 2F10.3, 2F6.3, F5.0),

where the first three words denote the day, month, and year, respectively, the next word represents the time (EDT), the next two words give the latitude (^{o}N) and longitude (^{o}W) of the lower left corner of the grid cell, the next two words represent the fractional coverage of all clouds and cumulus clouds, respectively, and the last word denotes the average cumulus cloud top height (hundreds of feet). Note that a cumulus cloud top height of -999 signifies that no cumuli were present, or that pixels with cumuli also were contaminated by other cloud types. The format of the second record is:

(1X, 40I3).

The integers in this records represent the number of satellite data elements that fell within a given category. The words in this record correspond directly with the height classes described above.

Special Conditions--

The visible and infrared images for 1600 EDT on July 30, 1983 had data quality problems and could not be processed. No statistics were provided for that time. In addition, the rawinsonde data for 0000 GMT on August 17, 1980 were not available. Cloud top height statistics for August 16, 1980 were calculated using the nearest 1200 GMT rawinsonde data, as discussed in Section 2.2.

2.4.4 Task 3

Output Specifications--

The output for Task 3 is on files 44 through 67 of Tape 4, and on Tapes 5, 6, and 7. Table 3 shows the dates, times, and regions analyzed. The areas for which gridded output is provided are quite large for Task 3, resulting in a need to break up the output into many sectors. Also, the regions studied for August 7 and August 8 are somewhat different from those studied for August 9, 10, and 11. As a

result of these considerations, the sectors shown in Figure 7 were defined. The frequency distribution of cloud top heights also is included with the results of Task 3.

Format—

The format of the output for Task 3 is the same as for Task 2.

Special Conditions—

The entire satellite image for August 8, 1980 at 1600 EDT could not be decoded by the IRIS, and no statistics have been produced for that time. Also, sector 1S (see Figure 7a) could not be processed for 2200 EDT on August 8, 1980. There also were data quality problems with the 1300 EDT and 1600 EDT images on August 10, 1980. Severe noise and missing records did not allow CSU to produce statistics north of 39.49°N or south of 35.8°N at 1300 EDT, and north of 40.0°N or south of 35.36°N at 1600 EDT.

A minor, but persistent, problem occurred with all of the satellite data for cases comprising Task 3. Since the grids for those cases covered quite a large area, the visible channel satellite data were ordered from NOAA/EDIS in two sections (i.e. an eastern and a western section). Although it was requested that a spatial overlap between the sections be provided by NOAA/EDIS, the data received at CSU contained no such overlap. The result was that a small number of grid cells were split between the image sections. No output for those grid cells could be produced by CSU. The exact geographic location of the missing output varied from one image time to another depending on the precise details of the navigation of the data and the manner in which the data files were produced at the University of Wisconsin.

Finally, no rawinsonde data were available for 0000 GMT on August 10, 1980. Cloud top height statistics for August 9 were computed using the nearest 1200 GMT rawinsonde data.

2.4.5 Task 4

Output Specifications—

The output for Task 4 is contained on Tape 2. The contents of that tape are shown in Table 4, along with the dates, times and regions analyzed. Because of the size of the area analyzed, the output data are provided for an eastern and a western sector. These sectors are depicted in Figure 8. The frequency distribution of cloud top heights also is included with the results of Task 4. Note that the output files for 2300 EDT on July 28, 1981 are at the end of Tape 3, rather than on Tape 2.

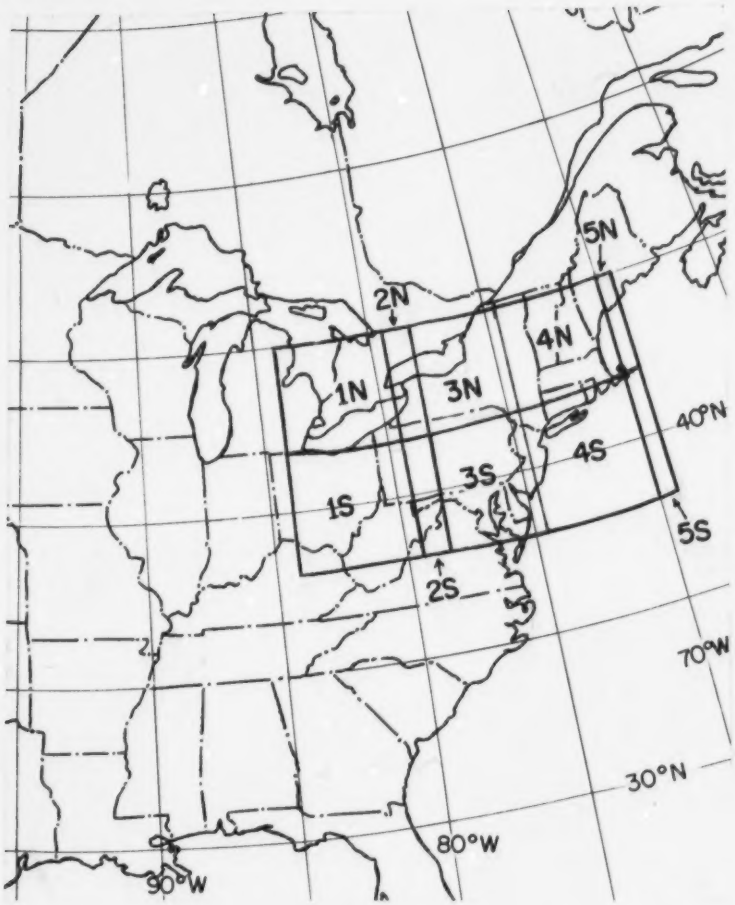

(a)

Figure 7. Regions covered by grids for Task 3. (a) represents grid for August 7, 8, 1980, (b) is grid for August 9, 10, 11, 1980. Sector identifiers are shown.

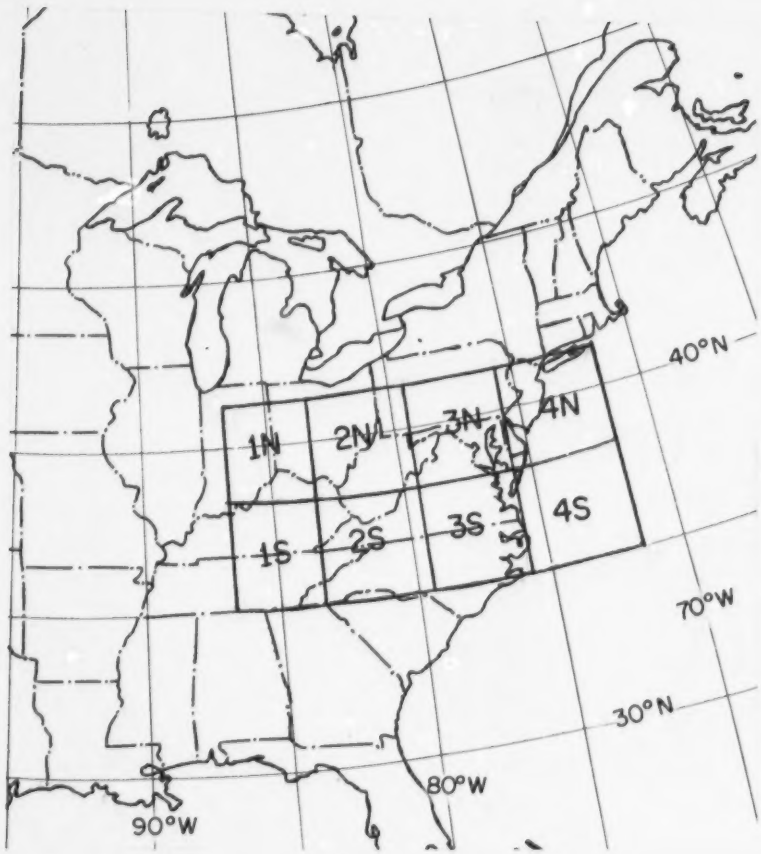

(b)

Figure 7. Continued

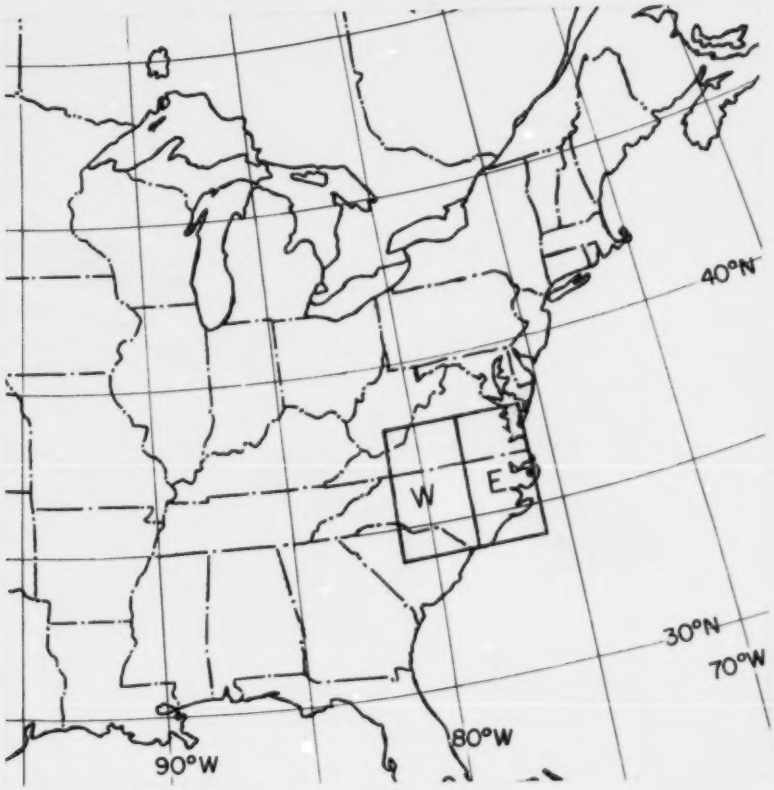

Figure 8. Region covered by grid for Task 4. Western (W) and Eastern sectors are shown.

Table 4
Output for Task 4

Tape #	File #	Date/Hour (EDT)		Sector
2	1	7/22/81	1200	East
	2		1200	West
	3		1300	East
	4		1300	West
	5		1400	East
	6		1400	West
	7		1500	Northeast
	8		1500	Southeast
	9		1500	Northwest
	10		1500	Southwest
	11		1600	East
	12		1600	West
	13		1700	East
	14		1700	West
	15		1800	East
	16		1800	West
	17		1900	East
	18		1900	West
	19		2000	East
	20		2000	West
	21		2100*	East
	22		2100*	West
	23		2200*	East
	24		2200*	West
	25		2300*	East
	26		2300*	West
	27	7/28/81	1200	East
	28		1200	West
	29		1400	East
	30		1400	West
	31		1500	East
	32		1500	West
	33		1600	East
	34		1600	West
	35		1700	Northeast
	36		1700	Eastcentral
	37		1700	Southeast
	38		1700	Northwest
	39		1700	Westcentral
	40		1700	Southwest
	41		1800	East
	42		1800	West
	43		1900	East
	44		1900	West
	45		2000	East
	46		2000	West

*from IR data only

Tape #	File #	Date/Hour (EDT)	Sector
	47	2100*	East
	48	2100*	West
	49	2200*	East
	50	2200*	West

*from IR data only

Format--

The format of the output for Task 4 is the same as for Task 2.

Special Conditions—

The image for 1300 EDT on July 28, 1981 was unavailable, and no statistics were produced for that time. Missing data records caused difficulties with processing two other image times. In order to avoid the gaps in the data, the output for the times in question was broken into several sectors. The output for 1500 EDT on July 22, 1981 was supplied in four sectors, whereas the output for 1700 EDT on July 28, 1981 was given in six sectors.

SECTION 3
CONCLUSIONS AND RECOMMENDATIONS

The work reported here has demonstrated the viability of deriving total cloud amount, cumulus cloud amount, and cumulus cloud top height statistics from digital GOES data. The interactive technique developed at CSU allowed the rapid processing of large quantities of satellite and rawinsonde data in order to accomplish that goal. The successful execution of the contracted tasks is significant in that it should allow the EPA model, into which the current results are to be entered, to perform a more accurate and comprehensive simulation of air pollution than has been accomplished previously. The true worth of the work reported here must be determined by the improvement that the cloud field analyses cause in the EPA model.

There are several additional tasks that should be executed in order to enhance the usefulness of satellite data for modelling air pollution. The first of these tasks is a comparison of the satellite-derived statistics with statistics derived from other data platforms. A comparison of cumulus cloud top heights derived from aircraft-borne LIDAR data and from GOES data is to be performed by CSU and EPA scientists in the near future, with the results to be published as a scientific journal article. That study should partially satisfy the need for intercomparison.

A second desirable accomplishment would be to further investigate the impact of cirrus clouds on the calculated cloud statistics. In particular, the effect of the transmittance and emittance of cirrus on satellite-derived cumulus cloud top temperatures requires further research. Although Reynolds and Vonder Haar (1977) and others have addressed this problem, it still is far from solved.

Many other applications of satellite data to the concerns of the EPA also are possible. For instance, the vertical velocities of convective clouds may be inferred from satellite data in order to provide details of pollutant transport. Also, the motions of small cumuli may be observed by satellite in order to quantitatively diagnose horizontal transport processes. Similarly, features within the atmospheric moisture field may be followed using multispectral satellite data. The pursuit of these applications could prove beneficial to the EPA, or to others interested in the air pollution problem.

REFERENCES

Adler, R. G., and M. J. Markus, 1982: Determination of thunderstorm heights and intensities from GOES infrared data. Preprints, 9th Conference on Weather Forecasting and Analysis (Seattle), AMS, Boston, 250-257.

Barnes, S. L., 1964: A technique for maximizing details in numerical weather map analysis, J. Appl. Meteor., 3(4), 396-409.

_____, 1973: Mesoscale objective map analysis using weighted time-series observations. NOAA Tech. Memo. ERL-NSSL-62, Norman, Oklahoma, 60 pp.

Desbois, M., G. Seze, and G. Szejwach, 1982: Automatic classification of clouds on METEOSAT imagery: Application to high-level clouds. J. Appl. Meteor., 21, 401-412.

European Space Agency, 1980: METEOSAT system guide, Vol. 5, Meteorological Products (G. C. Bridge, Ed.), METEOSAT Management Dept., ESOC, Darmstadt, FRG.

Kivel, B., 1978: Theoretical studies for improving atmospheric transmittance models used in analysis of satellite infrared data. Report to NOAA/NESS under Contract No. 7-35253, 50 pp.

Lamb, R. G., 1983: A regional scale (1000 km) model of photochemical air pollution. Part I: Theoretical formulation. EPA, Environmental Sciences Research Lab., Research Triangle Park, NC.

Pitts, D. E., W. K. Reeser, and M. A. Mendlowitz, 1975: Equivalent blackbody temperature of the top of a severe storm. J. Appl. Meteor., 14, 609-618.

Reynolds, D. W., and T. H. Vonder Haar, 1977: A bispectral method for cloud parameter determination. Mon. Wea. Rev., 105(4), 446-457.

APPENDIX A

Description of the Interactive Research Imaging System (IRIS) at Colorado State University

The IRIS is a multi-purpose image processing and computational system geared towards research and development in the Atmospheric and Earth Sciences, with particular emphasis on digital satellite imagery. The total system will be discussed according to the following five subtopics:

1. Computer Hardware and Peripherals
2. Video Display Hardware and Peripherals
3. Communications Between Systems
4. System Executive Software
5. Applications Software

Reference Figure 1 for the current configuration of CSU's Department of Atmospheric Science Direct Readout Satellite Earth Station.

I. Computer Hardware and Peripherals

Figure 1 represents the present configuration of CSU's Department of Atmospheric Science Direct Readout Satellite Earth Station. It consists of five separate Central Processor Units (CPUs) which are interconnected via communication lines.

The DEC VAX 11/780 is the main processor to be used for all research and data handling. The VAX 11/780 features a 32-bit architecture, efficient memory management, and a virtual memory operating system. These features provide the user with the illusion of unlimited memory space. The processor includes three megabytes of MOS memory and an 8K byte write-through memory cache which results in a 290-nanosecond memory access time. Memory management includes four hierarchical processor access modes, used by the operating system to provide read-write page protection between user software and system software. Peripherals on the VAX include two disk drives, two tape transports and a DECwriter III. The disk drives are RM05s; they are 300 megabyte drives offering an average seek time of 30 ms and an average rotational latency of 8.33 ms. The TU77s are 125 IPS, 300/1600 BPI tape transports. The DECwriter III is used as the system console and consists of a keyboard and a hardcopy printer.

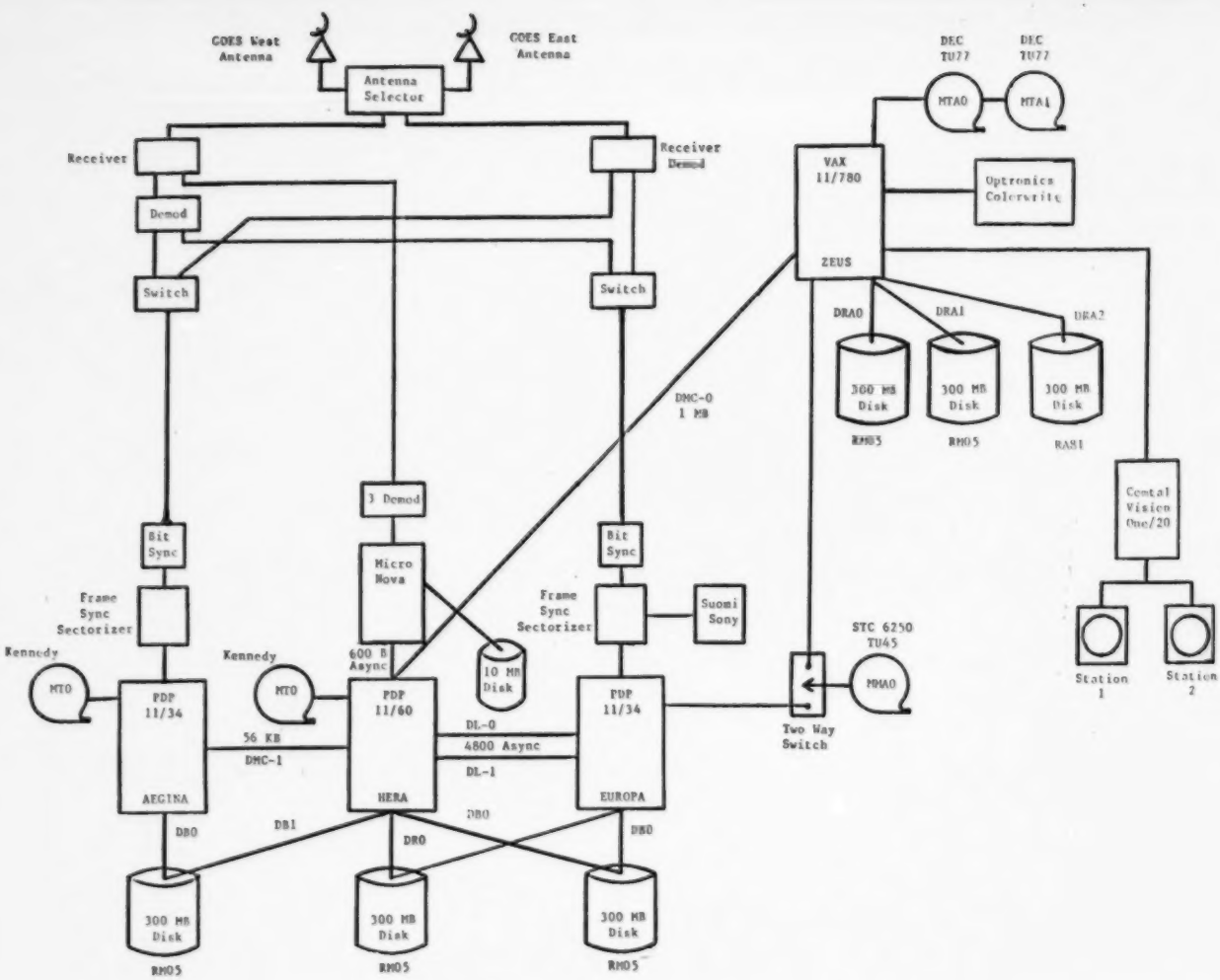

Figure 1. Configuration of the IRIS-DRSES computer system.

The DEC PDP 11/60 will be used primarily as a communications frontend processor. The 11/60 is a 16-bit machine. The processor has a 2K byte cache which results in an effective memory cycle time of 550 nanoseconds. It includes 128K bytes of MOS memory with backup and also has a Floating Point Processor. Peripherals on the PDP 11/60 include a DECwriter II, 30 CPS console; a Kennedy #9300 125 IPS, 800/1600 BPI tape transport; a Digi-Data 45 IPS, 1600 BPI tape transport; and a Control Data Corporation #9766 300 megabyte disk drive, offering an average seek time of 30 ms and an average rotational latency of 8.33 ms.

There are two DEC PDP 11/34's. Each 11/34 has 128K of MOS memory, a memory management system which provides protection andd relocation features for multiuser applications, and a DECwriter console. In addition to each of the above, the Earth Station's 11/34 has 2K bytes of cache, a battery backup, a Control Data Corporation #9766 300 megabyte disk drive, offering an average seek time of 30 ms and an average rotational latency of 8.33 ms, and a Kennedy #9300 125 IPS, 800/1600 BPI tape transport.

The last CPU we have in the house is a Data General Micro-Nova. The Micro-Nova has 32K bytes of memory and runs under data General's DOS operating system. Peripherals on this system include a 10 megabyte disk drive, two 32 hard sector 8' floppy drives, and a Teletype #43 used as the system console.

II. Video Display Hardware and Peripherals

The COMTAL Vision One/20 system is used for image processing. The two user stations on the COMTAL allow users to communicate with the COMTAL and the VAX. Station 1 consists of a CRT connected to the VAX, a keyboard, a high resolution monitor, and a data tablet. Station 2 consists of a CRT connected to the VAX, a keyboard, a high resolution monitor, track-ball, and video camera/light table. Seven image planes and eight graphics planes are available to be shared between the two stations. An image plane is 512 X 512 X 8 pixels; a graphic plane is 512 X 512 X 1. The refresh rate is 1/30 sec. The video camera/light table allows for digitizing of photographs, slides, overlays, etc. Available options on the COMTAL include refresh memory, image combination and convolution, histogram and statistical processor, image classifier, and independent small area processor. Due to the extensive capabilities of the COMTAL Vision One/20, please refer to the COMTAL Vision One/20 User's Manual for details.

III. Communications Between Systems

Two major types of communications exist in our system. Reference Figure 1. The first type are those lines which connect CPU to CPU. There are six such lines presently. The four lines between the VAX, 11/60, and the 11/34's are DECnet links. The line between the Micro-Nova and the 11/60 is an RS232 line and, finally, there is a link between the VAX and the COMTAL. The speeds of these lines are noted in Figure 1.

The second form of communication is accomplished by allowing a CPU to access a disk, other than its own, directly rather than by going through the DECnet line. Reference Figure 1 for this dual-ported disk scheme.

IV. System Executive Software

The operating system for both PDP 11/34's and 11/60 is DEC's RSX 11-M, version 3.2. The VAX is operating under DEC's VMS, version 3.0. RSX 11-M has been modified slightly to provide for systems tailored more to our needs than originally developed.

V. Applications Software

The Micro-Nova is used to collect and archive data from data collection platforms (DCP's) located in the area covered by the GOES East and GOES West satellites. These data can be accessed by the 11/60 using software developed in-house.

An extensive set of software has also been developed to run on the VAX 11/60, and 11/34's. This software will provide the means to:

1. Collect satellite data to tape or disk
2. Sectorize satellite data
3. Display image data
4. Navigate image data
5. Enhance or further process image data
6. Provide data to the COMTAL via the VAX

APPENDIX B

DIGITAL SATELLITE DATA INTERPRETATION

The power received at the satellite is expressed as

$$P_{r\lambda} = N_{s\lambda} A_c \frac{\pi\alpha^2}{4} \qquad \text{(D1)}$$

where $N_{s\lambda}$ is the measured spectral irradiance, A_c is the area covered by the aperture of the radiometer, and α is that aperture (in radians), as in Figure D1.

Within the radiometer, this power is converted to a voltage

$$V_o = f(P_r), \qquad \text{(D2)}$$

where f is a known calibration function.

Finally, the voltage is converted to a digital count via

$$C_D = g(V_o), \qquad \text{(D3)}$$

where g is a known digitizing function. The digital count C_D is received at the satellite earthstation.

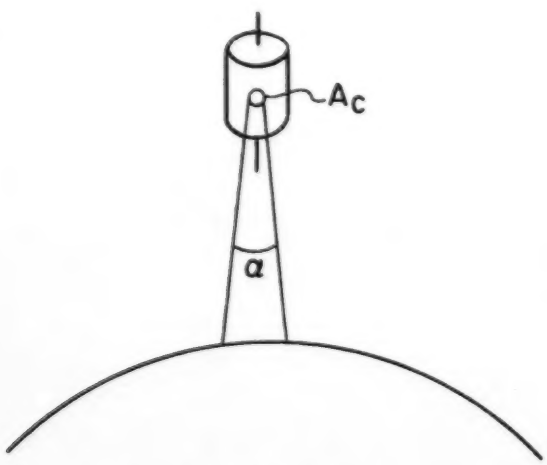

Figure D1: Satellite viewing geometry